

## Article

# A New Earth Observation Service Based on Sentinel-1 and Sentinel-2 Time Series for the Monitoring of Redevelopment Sites in Wallonia, Belgium

Sophie Petit <sup>1,\*</sup>, Mattia Stasolla <sup>2</sup>, Coraline Wyard <sup>1</sup> , Gérard Swinnen <sup>1</sup>, Xavier Neyt <sup>2</sup> and Eric Hallot <sup>1</sup>

<sup>1</sup> Remote Sensing and Geodata Unit, Institut Scientifique de Service Public (ISSEP), 4000 Liège, Belgium; c.wyart@issep.be (C.W.); g.swinnen@issep.be (G.S.); e.hallot@issep.be (E.H.)

<sup>2</sup> Signal and Image Centre, Royal Military Academy, 1000 Brussels, Belgium; mattia.stasolla@rma.ac.be (M.S.); xavier.neyt@rma.ac.be (X.N.)

\* Correspondence: s.petit@issep.be

**Abstract:** Urban planning is a challenge, especially when it comes to limiting land take. In former industrial regions such as Wallonia, the presence of a large number of brownfields, here called “redevelopment sites”, opens up new opportunities for sustainable urban planning through their revalorization. The Walloon authorities are currently managing an inventory of more than 2200 sites, which requires a significant amount of time and resources to update. In this context, the Sentinel satellites and the Terrascope platform, the Sentinel Collaborative Ground Segment for Belgium, enabled us to deploy SARSAR, an Earth observation service used for the automated monitoring of redevelopment sites that generates regular and automatic change reports that are directly usable by the Walloon authorities. In this paper, we present the methodological aspects and implementation details of the service, which combines two well-known and robust methods: the Pruned Exact Linear Time method for change point detection and threshold-based classification, which assigns the detected changes to three different classes (vegetation, building and soil). The overall accuracy of the system is in the range of 70–90%, depending on the different methods and classes considered. Some remarks on the advantages and possible drawbacks of this approach are also provided.

**Keywords:** automatic monitoring; time series; change detection; Sentinel-1; Sentinel-2; urban planning



**Citation:** Petit, S.; Stasolla, M.; Wyard, C.; Swinnen, G.; Neyt, X.; Hallot, E. A New Earth Observation Service Based on Sentinel-1 and Sentinel-2 Time Series for the Monitoring of Redevelopment Sites in Wallonia, Belgium. *Land* **2022**, *11*, 360. <https://doi.org/10.3390/land11030360>

Academic Editor: Sara Venafra

Received: 28 January 2022

Accepted: 25 February 2022

Published: 1 March 2022

**Publisher’s Note:** MDPI stays neutral with regard to jurisdictional claims in published maps and institutional affiliations.



**Copyright:** © 2022 by the authors. Licensee MDPI, Basel, Switzerland. This article is an open access article distributed under the terms and conditions of the Creative Commons Attribution (CC BY) license (<https://creativecommons.org/licenses/by/4.0/>).

## 1. Introduction

In former industrialized regions characterized by a large number of brownfields and a high population density, such as Wallonia (the southern region of Belgium), offering new living spaces while limiting land take has become a challenge. The management of vacant lands is then a key to urban planning, as monitoring abandoned sites can support policy and decision-making [1]. In Wallonia, many industrial sites were developed during three distinct periods between the end of the 18th century and the middle of the 20th century. However, since the middle of the 20th century, industrial sites have been increasingly abandoned, first due to the closure of coal mines, then of manufacturing and metallurgical industries. Moreover, a phenomenon of relentless de-urbanization has increasingly emptied the urban centers. This has led to the development of industrial and urban wastelands, which, depending on their origin, can vary in size from a few dozen square meters to a few dozen hectares (e.g., coal mines or blast furnaces), with 75% of them being less than one hectare. As the vast majority of these sites are located in urban areas, they negatively impact the urban fabric but also represent an opportunity for sustainable urban planning as they can be revalorized, with their reuse being a fundamental asset in land management [2]. Therefore, the Walloon authorities have proposed a detailed definition for those sites and have catalogued them into an exhaustive inventory [3,4]. The redevelopment sites (RDSs) are thus defined as “property or group of properties that have been or are intended

to be used for an activity, excluding housing, and whose current state is against land management best practices, or constitutes a deconstruction of the urban fabric" [5]. The RDS inventory, which enables potential investors and public authorities to find out about vacant land and its condition, currently contains more than 2200 sites and is available online [6]. Updating it is essential to keep a record of all the sites that have already been enhanced and provide reliable information to the actors consulting the database. Currently, this update is performed, on the one hand, by the visual analysis of orthophotos annually provided, as open data, over the entire Walloon territory and, on the other hand, by systematic field visits. These methodologies are time-consuming and costly. Indeed, the first solution requires several months of work for the analysis of all the RDSs included in the inventory; moreover, the results can only be provided once a year, and there is also a delay between the moment of data acquisition and their availability. As for the second solution, the systematic field visits, the analysis is spread over several years. However, the Walloon authorities estimate that less than 10% of the RDSs are likely to be redeveloped from one year to the other and show major changes (the three classes of interest for the administration are buildings, vegetation and soil). It is, therefore, necessary to find a way to reduce the time spent on the inventory update by providing operators with a list of sites presenting indications of significant changes that would enable them to concentrate their efforts on these sites. The problem of how to efficiently monitor redevelopment areas (usually called brownfield sites or more generally, vacant lands, although with a slightly different meaning than ours) has been examined in many studies that mostly focus on either their potential for policy-makers by using GIS data [7] or the detection of new vacant lands. In particular, remote sensing data have been used in several studies for the detection of new brownfields: Ref. [8] investigated the potential of IKONOS data in the object-oriented classification approach and Ref. [9] investigated IKONOS, QuickBird and hyperspectral data. In a recent study [10], the fusion of remote sensing images thermal data, GIS layers and citizen science data is proposed for the identification of urban vacant land. Remote sensing is also used, at a fine scale, for the detection and monitoring of hazardous substances and materials, as shown in [11].

Change detection is one of the major applications of satellite-based remote sensing data [12], and many different satellite-based change detection methods have been developed and used in recent decades. Among the most commonly used methods are algebra methods (e.g., Image Differencing, Ratioing or Change Vector Analysis), transformation-based methods (e.g., Principal Component Analysis), classification-based methods [13] and time series analysis. In [14], the authors provide a review of the different techniques, a guide to compare them by placing a clear separation of variables between the analysis unit and classification method and report that pixel and post-classification change methods remain the most popular choices. The review also presents some advantages and limitations of the different techniques. These limitations and how to overcome them have been widely studied and have led to more refined methodologies, e.g., super-resolution mapping and the analysis of mixed pixels for the improvement of land-cover class maps [15]. In addition, many other methods have recently been developed, notably based on artificial intelligence [16,17]. However, in [16], it was highlighted that supervised AI methods require massive training samples to obtain a robust model and that processing remote sensing big data requires a large amount of computational resources, which limits the implementation of the AI model. It is, therefore, crucial to choose the methodologies based, on the one hand, on needs such as the scale of the application and the thematic objectives and, on the other hand, on aspects such as the resolution of the available images and their ability to provide the required comparison features [14]. In the framework of this project, we opted for a time series analysis approach as, depending on the method, it offers a number of advantages, e.g., being able to detect abrupt and gradual changes (BFAST) or to capture subtle but consistent trends (LandTrendR), Continuous Change Detection and Classification (CCDC) being able to detect a variety of LULC changes continuously with high spatial and temporal accuracies [18]. However, in [18], the limitations of these methods are also presented,

e.g., time-consuming, requiring many resources, unsuitable for irregular observations, and some are unable to identify types of changes. It is, therefore, crucial that the choice of time series analysis method takes into account the objective of the research, and considers the need to find the change points as soon as possible in real-world applications and that there is a detection delay for many existing approaches [19,20].

Within this context, the European Copernicus program has opened, with the launch of Sentinel-1 and Sentinel-2 satellites, new opportunities thanks to their high spatial and temporal resolution. The Sentinel-1 mission consists of a constellation of two polar-orbiting satellites mounting a C-band synthetic aperture radar (SAR) imaging system. They offer a repeat cycle of six days and all-weather and day-and-night monitoring capabilities [21]. The two Sentinel-2 satellites A and B are characterized by a sun-synchronous orbit, phased at 180 to each other, and a repeat cycle of 5 days [22]. The temporal resolution of the Sentinel satellites ensures enough data to create time series [23–25], and their spatial resolution allows for the identification of landscape features [26] and monitoring urban areas [27], whereas the Sentinel-2 spectral resolution facilitates the thematic identification of land cover [28–30].

In addition to the use of SAR and optical data separately, the combination of SAR and optical data has been highlighted in domains such as vegetation monitoring [31] and urban mapping [32,33]. Combining the two types of data has the advantage of coupling features and thus overcoming some limitations, such as clouds, shadows and snow cover for the optical data. Regarding the Sentinel images, the combination has been investigated in various domains, such as forest disturbance [34], soil tillage [35] and urban mapping [36]. In [37], the use of Sentinel-1 data alone, Sentinel-2 data alone and their combined use for forest–agriculture mapping are compared.

The demand for automated operational services providing near-real time information for environmental monitoring has increased substantially in recent years, and several studies have investigated their feasibility and proposed possible implementations, mainly for natural events monitoring. In [20], the Thresholding Rewards and Penances TRP concept was applied for a near-real time forest disturbance alert system based on PlanetScope imagery, producing new forest change maps when a new image is made available. They proposed a robust statistical method to estimate forest clear-cuts, but the use of PlanetScope images makes the service costly as they need to acquire raw imagery. In [38], a near-real time automatic avalanche monitoring system based on Sentinel-1 data was presented, and an age tracking algorithm was developed, while, in [39], the focus was on burned forest areas using Sentinel-2 data. For mapping burned areas, the latter used a selection of spectral indices to compare the pre-fire and post-fire values. In [40], an automatic and repeatable plot-based change detection method, based on pre and post event Sentinel-1 and Sentinel-2 data, was designed and tested to map extreme storm-related damages. Most of the services are in the test or pre-operational phase and focus on localizing one type of change, with hindsight of events and/or using one type of remote sensing data being sometimes costly.

The goal of this paper is to present the methodological aspects and implementation details of SARSAR, a new Earth observation service for the monitoring of redevelopment sites in southern Belgium. For its deployment, a number of requirements made by the Walloon administration had to be met, namely: (i) the implementation of a straightforward automatic operational tool providing results on a regular basis (once every two months); (ii) the ability to detect changes in vegetation, buildings and soil, on a set of sites spread throughout the region's territory; (iii) the use of open-source data.

Differently from other methodologies and services mentioned above, the focus is, therefore, on providing a response to the administration need of monitoring RDSs on a regional scale and identifying the time and type of change at the site level using free and open-source technology. In brief, by exploiting Sentinel-1 and Sentinel-2 data, the service automatically detects and characterizes changes in user-defined sites of interest and provides a final change list that can be directly used by the Walloon authorities to prioritize their daily work and reduce the time needed for the inventory update.

To fulfil the free and open-source technology requirement, we exploited Terrascope, the Belgian contribution to the Sentinel Collaborative Ground Segment (CollGS), which provides access to pre-processed Sentinel data [41] and computer capacity for the execution of the process and its automation. The Sentinel Collaborative Ground Segments were created by ESA and its Member States to facilitate the access to the Sentinel data and the data exploitation. CollGS can be used for various applications, as shown by Ref. [42], who used Terrascope for geohazard monitoring.

To be able to provide a list of the RDSs that are likely to change, several steps were implemented. Considering the number of sites to be processed and the fact that aggregate information is needed for each RDS, we opted for an object-based approach. Moreover, since the number of training samples required to implement a solution based on AI would have been prohibitive, our final choice was a combination of unsupervised methodologies.

After data preparation, where the extraction of temporal features from the Sentinel time series was performed, two processes were run: first, the change point detection analysis based on the Pruned Exact Linear Time (PELT) [43], whose goal is to flag each site as changed/unchanged and to provide an estimate of the change date(s) [44] and then a rule-based classification based on threshold selection to characterize the types of changes.

Change point analysis is largely employed for the study of time series in many application domains, yet it is still underexploited within the remote sensing community, due to the fact that high resolution images were not easily accessible until a few years ago. In regard to our service, change point detection was chosen because it serves a twofold purpose: it directly provides an estimate of the date of change, which alone constitutes valuable information for the administration, and allows us to restrict the time window within which the change classification should be performed. As regards threshold selection, it is a common procedure in algebra-based change detection [45]. The selection of the best threshold could be associated with a priori knowledge or derived from the histogram of the image [12]. The advantage of thresholding is that it can guarantee a robust near real-time approach based on fast and automated processing [34]. To the best of our knowledge, there have not been other attempts to use change point detection in combination with threshold-based classification for the characterization of changes in urban areas.

The paper is organized into five sections: The Materials section presents the study area, the Sentinel data used for this study via the Terrascope platform and the ground truth used for validation. The Methods section is divided into three parts: the first part explains the feature extraction and the creation of temporal profiles, the second part investigates the change detection method chosen and the third part presents the methodologies used for the classification of the changes. The last three sections are the presentation of the results, the discussion and the conclusions.

## 2. Materials and Methods

### 2.1. Materials

#### 2.1.1. Study Area

The study was performed in Wallonia, the southern part of Belgium that covers an area of about 17,000 km<sup>2</sup>. The industrial development in this region took place mainly along the Haine–Sambre–Meuse–Vesdre river axis. In total, slightly over 2200 sites are distributed mainly along this particular path, for a total area of 3800 hectares (Figure 1). However, a certain number of sites are spread over the whole territory of Wallonia. As mentioned in the Introduction, the size of the RDSs themselves, depending on their original use, can vary greatly. Figure 2 shows a former industrial area presenting a large number of RDSs of different sizes.

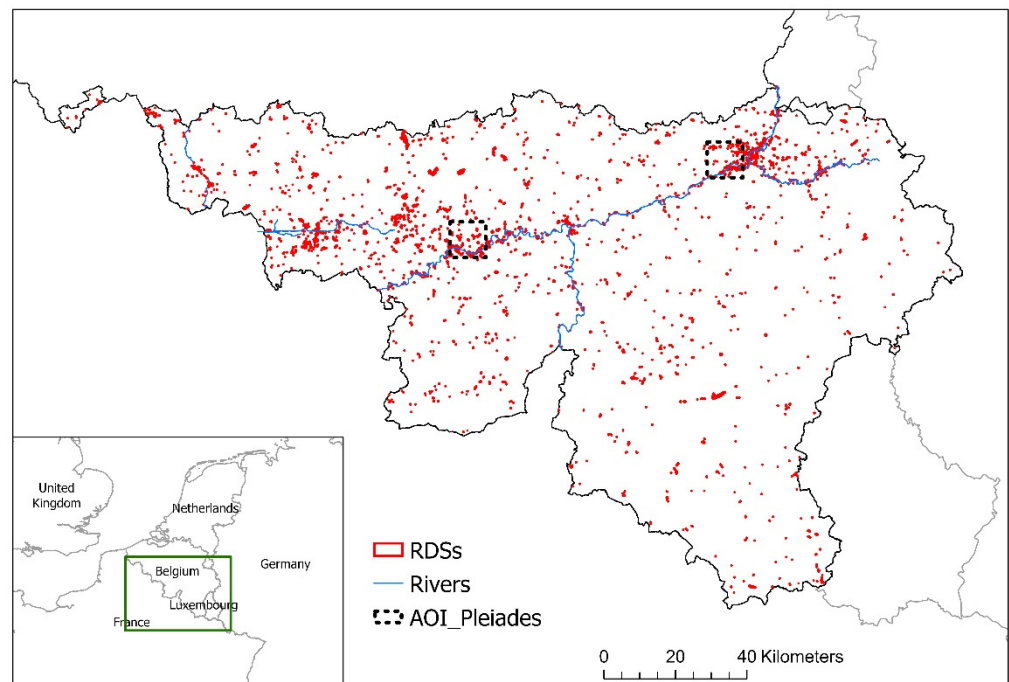


**Figure 1.** Study area (green mark), with the spatial distribution of the RDSs in Wallonia (red marks) and the Pléiades ground truth areas (black marks).



**Figure 2.** Close-up, illustrated with an orthophoto, of a former industrial area presenting several RDSs of different sizes.

### 2.1.2. Sentinel Data and Computing Environment

Sentinel-1 and Sentinel-2 data have been available since 2014 and 2015, respectively. Both missions consist of two satellites (A and B). Sentinel-1 mounts an SAR instrument that operates at a center frequency of 5.405 GHz and supports operation in dual polarization. For Belgium, the typical acquisition mode is Interferometric Wide (IW) in dual polarization

(VV+VH), which provides a resolution of around  $5 \times 20$  m for Single Look Complex (SLC) products and around  $20 \times 20$  m for Ground Range Detected (GRD) products [21]. Sentinel-2 carries an on-board Multi Spectral Instrument (MSI) measuring the reflected solar spectral radiances with 13 spectral bands ranging from visible to shortwave infrared (SWIR) bands [22]. The spatial resolution is 10 m, 20 m or 60 m depending on the spectral band. As regards the temporal resolution, Sentinel-1 and Sentinel-2 have a repeat cycle of 6 and 5 days, respectively, making them suitable for the creation of time series.

All the processing was carried out using the Terrascope platform [41], the Sentinel Collaborative Ground Segment for Belgium. Terrascope was chosen because it offers, in open access, up-to-date pre-processed Sentinel data, a computing environment, long-term maintenance and technical support. Concerning the Sentinel-2 data, the platform makes available atmospherically corrected images Level 2A Top-of-Canopy (TOC), downloaded from the ESA hubs. As regards Sentinel-1, along with the original SLC and GRD products, Terrascope also conveniently offers the corresponding calibrated and orthorectified images, which we ultimately used to avoid unnecessary pre-processing. Their spatial resolution is  $20 \times 20$  m resampled at 10 m. The SARSAR service was run on a dedicated machine with a 6-core hyperthreading enabled CPU, 24 GB RAM, a boot volume of 2 TB and a data volume of 8 TB. Data storage was ensured by a PostgreSQL (11.11) server. The data processing was performed via a combination of Python (3.6) scripts, PostgreSQL stored procedures and PostGIS (3.1) functions. The whole processing chain was launched automatically and at predefined intervals thanks to CRON. Ultimately, the final users received notifications and reports by e-mail.

### 2.1.3. Ground Truth

For validation purposes, two ground truth datasets were created by visual analysis. The first ground truth is based on the orthophotos (25 cm resolution) taken in summer 2016 and 2018, and focuses on the RDSs, spread throughout the region, for which there are changes that can be observed from Sentinel data. This dataset was developed to account for major changes and for which we do not have information about the exact dates of change. The second ground truth is based on Pléiades images (50 cm resolution) acquired monthly between January 2019 and December 2020 on two specific areas (Figure 1) with a high concentration of RDSs. This provides complementary information compared to the orthophotos' ground truth. In fact, while the orthophotos' ground truth focuses on RDSs with significant changes, this dataset was created to take into account in a more balanced way the different types of change. Although, due to meteorological conditions, only 14 and 16 images, respectively, are available for each area, an estimation of the change dates was extracted taking into consideration that several dates can occur per site. In addition to the change dates for the whole period, information on the changes occurring between summer 2019 and summer 2020 was also extracted in order to provide a dataset that complements the one based on orthophotos.

In total, 141 and 161 sites are present in the orthophotos and Pléiades ground truth, respectively. For each of the 302 RDSs, changes were manually recorded for vegetation, buildings and soil. Overall, 152 of the sites presented at least one change and 150 remained unaltered. The breakdown of the changes into the three possible types is shown in Table 1, and Figure 3 provides two examples of changes.

**Table 1.** Number of changes per ground truth and breakdown into change types.

Ground Truth	Building	Vegetation	Soil	Total Changes	Total RDSs
Orthophotos	60	97	125	282	141
Pléiades	8	13	15	36	161
Total	68	110	140	318	302



The proposed overall methodology, whose main goal is to provide a shortlist of the sites that are likely to have changed and for which an on-field visit would be required, is shown in Figure 4. The first main block is the feature extraction, where the Sentinel-1 and Sentinel-2 images available in Terrascope and described in the previous section are processed to obtain the above-mentioned temporal profiles of the RDSs (each RDS has multiple temporal profiles—one per feature). The second main block is devoted to the characterization of the changes, which is carried out in two steps: (i) the change detection, which flags a site as changed (or not) and provides an estimate of the change date(s)—this is carried out once every two months; (ii) the change classification, which is divided into two separated processes. First, when a change date is detected, a rule-based classification is performed in order to provide additional information on the type of change: vegetation, building or soil. Second, the same methodology is applied once per year, considering summer average features in order to detect gradual changes.

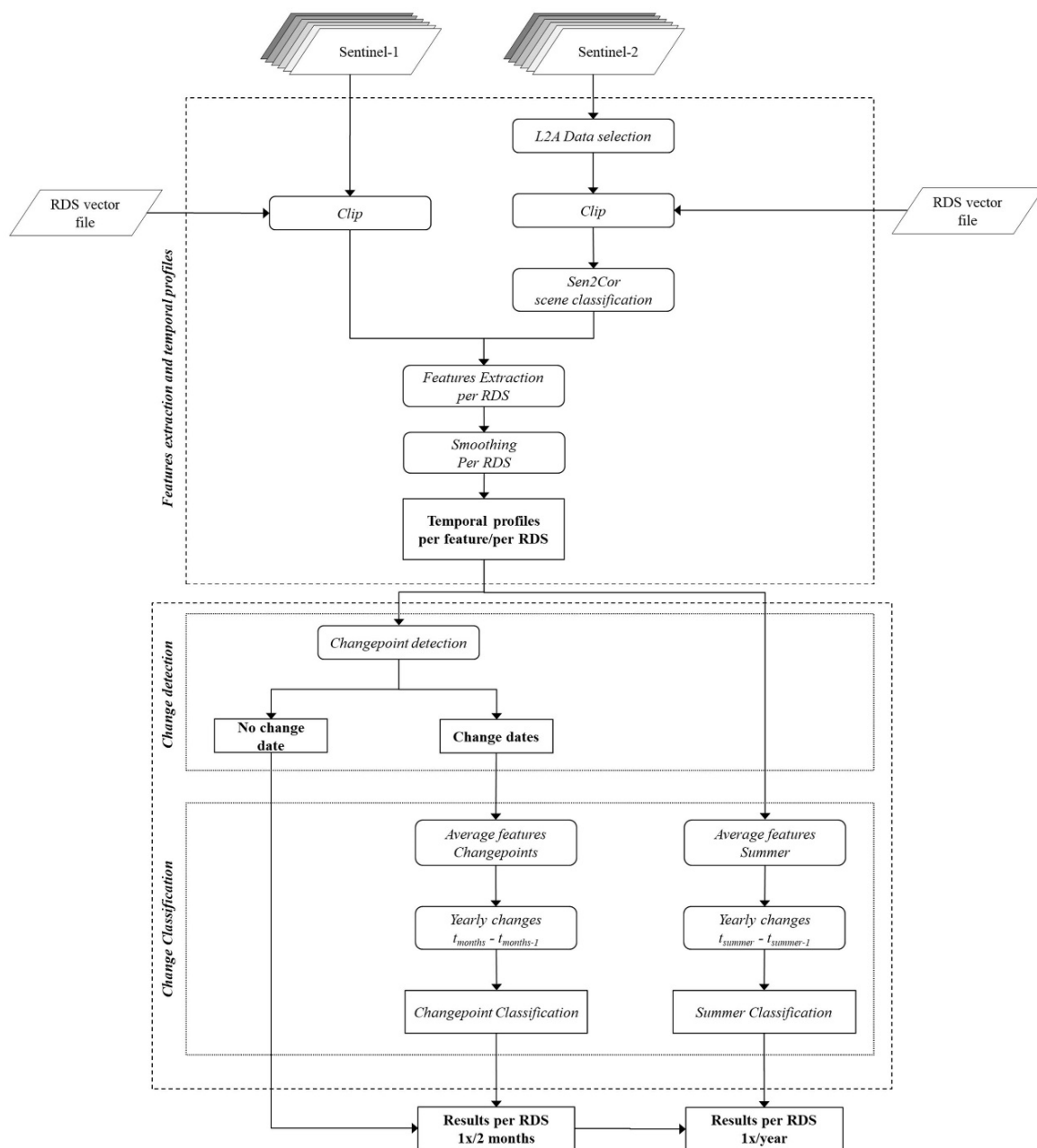


Figure 4. Workflow of the automatic change detection and classification of the RDSs.

The final output of the service is a csv file that is automatically delivered to the operator. For each RDS, this report includes: (1) information on whether a change has occurred or not, (2) the type of change and (3) the estimated date of the change (if available).

### 2.2.1. Features Extraction and Temporal Profiles

For each Sentinel-1 acquisition (more specifically, the VH band, which was found to be the most suitable for our scope) that contained the site of interest within the desired time frame, the average backscatter ( $\sigma_0$ ) for that site was computed and used to populate the corresponding temporal profile. Since a site can be typically seen from 3 to 4 different viewing angles (considering both ascending and descending orbits), separate profiles were created for each satellite pass and then averaged to obtain a unique “ $\sigma_{0VH}$ ” feature.

Regarding Sentinel-2 data, all the L2A tiles over the area were analyzed. Only the tiles presenting less than 25% of clouds were selected, which greatly reduced the number of undetected cloud pixels. Then, each image was clipped based on the RDS vector polygons file. Image co-registration was ensured during this process. Then, the Scene Classification layer, a classification map generated via the Sen2Cor ESA processor that accompanies every L2A image and is directly available in Terrascope, was used to remove every single pixel classified as “No\_Data”, “Cloud\_Shadows”, “Cloud\_Medium\_Probability”, “Cloud\_High\_Probability”, “Thin\_Cirrus” and “Snow”. This allowed us to remove, site per site, the dates for which no data, shadows, clouds, or snow pixels were present.

In the feature extraction step, six widely used spectral indices were calculated that were to be used in the next processes: (1) the Built-Up Areas Index (BAI) [47], (2) the Brightness Index (BI) [48], (3) the Second Brightness Index (BI2) [48], (4) the Normalized Vegetation Index (NDVI) [49], (5) the second Normalized Difference Water Index (NDWI2) [50] and (6) the soil brightness index (SBI) [47]. The selection of the spectral indices was motivated by their widespread application in the literature and by considering that most built-up indices require SWIR bands, which are available only in a coarse resolution for Sentinel-2. The BI2 index has been tested for built-up detection after applying NDVI and NDWI2 to mask vegetation and water [51]. BAI has proven to be useful to detect asphalt and concrete surfaces [47], and SBI has been successfully investigated by [47] and [52]. For each index, each RDS and each available image since 2015, the average per RDS was calculated and used to generate the Sentinel-2 time series:

$$BAI = ((B02 - B08)) / ((B02 + B08)) \quad (1)$$

$$BI = \sqrt{((B04 * B04) + (B03 * B03)) / 2} \quad (2)$$

$$BI2 = \sqrt{((B04 * B04) + (B03 * B03) + (B08 * B08)) / 3} \quad (3)$$

$$NDVI = ((B08 - B04)) / ((B08 + B04)) \quad (4)$$

$$NDWI2 = ((B03 - B08)) / ((B03 + B08)) \quad (5)$$

$$SBI = \sqrt{((B04 * B04) + (B08 * B08))} \quad (6)$$

where  $B0n$  corresponds to the  $n$ -th Sentinel-2 band used for the calculation, here  $B02$ ,  $B03$ ,  $B04$  and  $B08$ , all with a 10 m resolution.

To create the final temporal profiles (each RDS has multiple profiles, one per feature), a linear interpolation to fill in the gaps (1 data point per day) in the data and a smoothing using a Gaussian kernel with a standard deviation of 61 were performed.

### 2.2.2. Change Detection

The second processing block is the change detection, where some of the features extracted from the Sentinel images are jointly analyzed using the Pruned Exact Linear Time (PELT) [43]. The method is a well-known changepoint detection method that provides an exact segmentation of the time series with a linear time complexity.

Given a time series  $s = (s_1, \dots, s_k)$ , the number  $n$  and time position  $t_{1:n} = (t_1, \dots, t_n)$  of the changepoints are obtained by solving the following penalized minimization problem:

$$Q_n(s_{1:k}, p) = \min_{n, t_{1:n}} \left\{ \sum_{i=1}^{n+1} [C(s_{(t_{i-1}+1):t_i})] + p \right\} \tag{7}$$

where  $C$  is the segment-specific cost function

$$C(s_{a:b}) = \sum_{i=a+1}^b \|s_i - \bar{s}_{a:b}\|_2^2 \tag{8}$$

and  $p = \log(k)$  a penalty term to control overfitting.

In a preliminary study that we carried out on 22 test sites [44], we showed that the combined use of the Sentinel-1  $\sigma_{VH}$  and Sentinel-2 NDVI returns more accurate change detection results than those of the single features. Figure 5 shows an example of the changepoints detected on an RDS where a building was demolished between summer 2017 and summer 2018, and some vegetation grew between summer 2018 and summer 2019. As can be seen, the combined use of Sentinel-1 and Sentinel-2 detection successfully returned the two dates. After the optimization phase of the change detection process, during which we performed several tests on an extended dataset using different combinations of features, the NDVI feature was replaced by NDWI2.

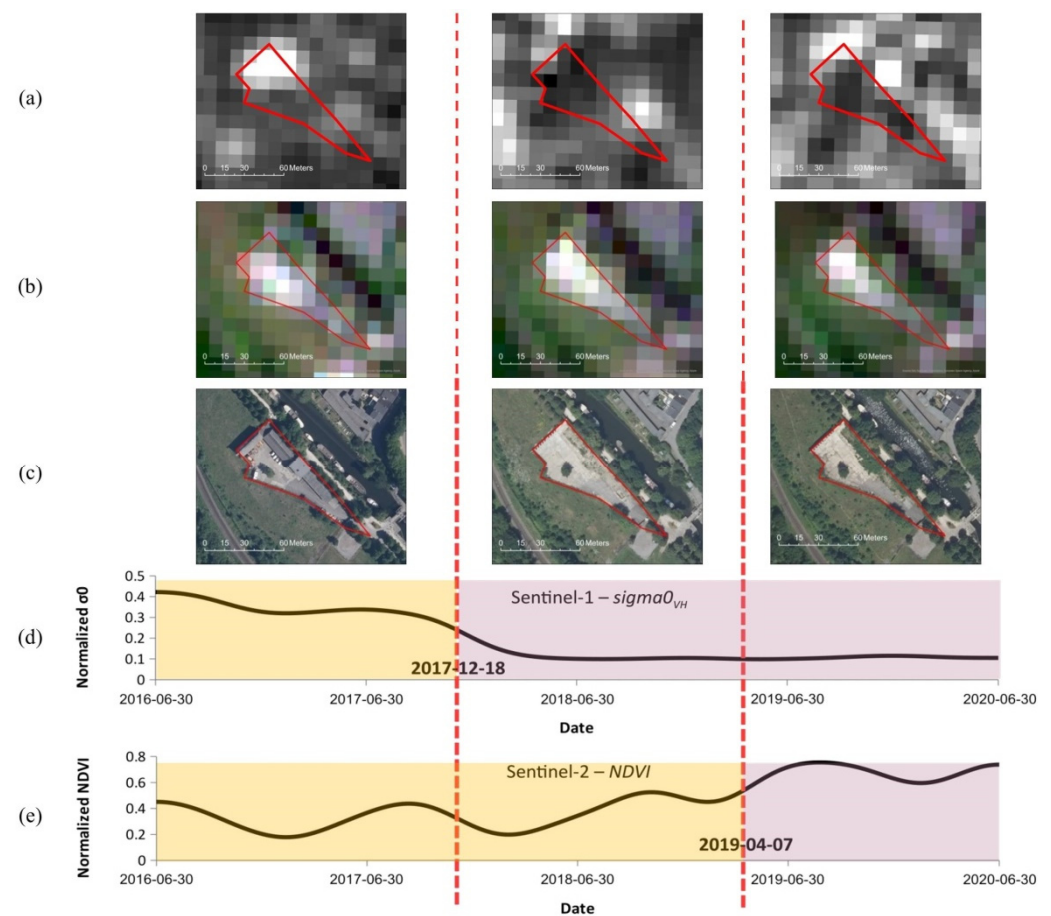


**Figure 5.** Changepoint analysis for the RDS “Service voirie d’Angleur” in Liège showing (a) Sentinel-1 image (left: July 2017; center: July 2018; right: July 2019); (b) Sentinel-2 images (left: July 2017; center: July 2018; right: July 2019); (c) orthophotos ground truth (left: summer 2017; center: summer 2018; right: summer 2019); (d) bi-dimensional time series  $\sigma_{VH}$  (Sentinel-1); (e) bi-dimensional time series NDVI (Sentinel-2).

The overall process returns either a list of changepoints dates (one or multiple) or no changepoints. When one or multiple changepoints are detected, these become the input of the next block—the change classification. When no changepoints are detected, this information is reported directly in the final report, “Results per RDS”.

### 2.2.3. Change Classification

Determining the type of changes is essential in providing information about the changes to the local authorities. The Sentinel-1  $\sigma_{VH}$  and Sentinel-2 indices temporal profiles were analyzed to determine suitable threshold boundaries that would represent a change for each land cover type (vegetation, building or soil), and the data from the ground truth datasets were used to validate the method. Thresholding-specific indices have been proposed and successfully applied in many studies [47,51], e.g., thresholding NDVI has been used to qualify land-cover change [53] and detect forest cuts [25]. The use of Sentinel-1 data, which is radar sensitive to variations in height and shape, allowed us to complement the information provided by the Sentinel-2 indices and improve the characterization of the changes to buildings.

For each site, two separate processes were considered that allow, on the one hand, to provide information on the type of change for progressive changes and, on the other hand, to classify the changes associated with the detected changepoints.

The first one is solely based on Sentinel-2 data. It focuses on the summer months ( $t_{summer}$ ), from May to August, as these are more appropriate for vegetation change. It also offers the best illumination conditions for the multi-spectral images considering the variation of the Sun–Zenith Angles due to the sensing time being the same throughout the year. This process, hereafter referred to as “summer classification”, offers the opportunity to detect changes that occur gradually over a one-year period. The second process, the “changepoint classification”, is based on both Sentinel-1 and Sentinel-2 features, and it is performed when one or multiple change dates are available from the previous block. It takes into account the average of the data available after the change date ( $t_{months}$ ), namely, 2 months for Sentinel-2 data and 1 month for Sentinel-1 data. A calculation of the distance between the average features of the time period from the year of the change ( $t_{summer}$  and  $t_{months}$ ) to the same time period the previous year (respectively,  $t_{summer-1}$  and  $t_{months-1}$ ) was performed. This distance was then compared to the thresholds of the different Sentinel-2 index and Sentinel-1 VH features in order to determine the chances of representing a type of change (Table 2). As described for the “summer classification”, the one-year time step for the “changepoint classification” was chosen in order to limit the influence of the illumination for Sentinel-2 and the seasonality effect. In addition, while the “summer classification” considered the average features from May to August, the “changepoint classification” takes into account 2 months for the Sentinel-2 indices and 1 month for the Sentinel-1 VH feature. This discrepancy in the number of months used is based on the fact that valid Sentinel-2 data are typically fewer due to cloud cover. On top of the change classification, NDVI and  $\sigma_{VH}$  helped us to determine the direction of the change (Table 2). Although the use of the VH band allowed this identification, the combination of the three indices, BI, BI2 and SBI, showed better results for the “summer classification”, which is why these indices were selected. The detailed workflow for the evaluation of the type of changes is shown in Figure 4.

**Table 2.** Rule-based classifier for the determination of the types of changes.

Change Classification	$t_{summer}-t_{summer-1}$	$t_{months}-t_{months-1}$
Vegetation increase	$NDVI \geq 0.1$	$NDVI \geq 0.1$
Vegetation decrease	$NDVI \leq 0.1$	$NDVI \geq -0.1$
Building change	$BI \geq 150$ or $BI2 \geq 150$ or $SBI \geq 250$	-
Building increase	-	$VH \geq 0.135$
Building decrease	-	$VH \geq -0.135$
Soil change	$BAI \geq 0.05$	$BAI \geq 0.05$

### 3. Results

#### 3.1. Change Detection

The performance was assessed in terms of true positive rate (TPR) and false positive rate (FPR). The overall problem can be in fact seen as a binary classification where either a “change” (1) or a “no change” (0) has to be detected. In order to compare the results with the ground truth, the latter was coded so that any change in any of the three classes (building, vegetation and soil) was assigned the value 1; in the case of no change for all three classes, the ground truth was given the value 0. A confusion matrix was then generated so that the number of true positives (TPs), true negatives (TNs), false positives (FPs) and false negatives (FNs) could be used to compute the TPR and FPR. To provide a unique measure that takes into account both detection and miss rates, the  $F_1$ -score was also calculated. For the sake of completeness, the overall accuracy (OA) is also reported.

It is worth mentioning that, due to the specific way in which the ground truth is constructed, in order to generate the confusion matrix, we made the arbitrary assumption that only one change per site occurred in the considered period of time. This is a simplification that helped us to compare the results in a more straightforward way, but might not fully reflect the real situation, especially for the sites belonging to the orthophotos ground truth, as for a certain number of them it is more likely that multiple changes occurred at different times.

The change detection was performed using the  $\sigma_{0VH}$  and NDWI features, which amongst the other features ultimately provided the highest accuracy. The use of both Sentinel-1 and Sentinel-2 data, which provide complementary information (the VH band mostly about buildings and the NDWI index mostly about vegetation and soil), allowed a more effective identification and classification of changes. The results for the entire dataset are shown in the first row of Table 3. The number of sites for which we had an estimated change is 108, 91 of which were correctly classified. Among the unchanged sites, we missed 46 of them, resulting in an OA of 79%. In terms of correct and miss detection rates, we, therefore, obtained a TPR of 66% and an FPR of 10%, with an  $F_1$ -score of 0.74.

**Table 3.** Change point analysis: confusion matrix and performance metrics.

	TP	FP	FN	TN	TPR	FPR	$F_1$ -Score	OA
Full dataset	91	17	46	148	66%	10%	0.74	79%
Pléiades	15	9	12	125	55%	7%	0.59	87%

In order to better understand the results of the following block, the change classification, it was helpful to separate the Pléiades detections from the full dataset. The results are provided in the second row of Table 1. For this dataset, the number of sites that were flagged as changed was 26, with nine FPs, whereas the correct detections of the unchanged sites were 125. As a result, the TPR and FPR decreased to 55% and 7%, respectively, and, consequently, the  $F_1$ -score dropped to 0.59. The OA, instead, increased to 87%, mainly due to the fact that the dataset was rather unbalanced.

#### 3.2. Change Classification

##### 3.2.1. Summer Classification

The “summer classification”, as we discussed in the previous section, takes into account, for each of the 302 sites, the summer comparison between 2016 and 2018 for the orthophotos dataset and between 2019 and 2020 for the Pléiades dataset. Again, the performance was assessed by combining the two datasets and computing the TPR, FPR and the  $F_1$ -score for each class, along with the overall accuracy (see Table 4). The overall performance of the yearly classification based on summer values is satisfactory. The best results were obtained for the “vegetation” class, for which the OA was 90% and the TPR and FPR were 87% and 9%, respectively. The resulting  $F_1$ -score was 0.80. The performance

for the “building” and “soil” classes were slightly lower, with an OA of 76% and 79%, respectively, yet still good, with an  $F_1$ -score above 0.7.

**Table 4.** “Summer classification” (full dataset): confusion matrix and performance metrics.

	TP	FP	FN	TN	TPR	FPR	$F_1$ -Score	OA
Vegetation	59	21	9	213	87%	9%	0.80	90%
Building	87	49	23	143	79%	26%	0.71	76%
Soil	103	26	37	136	74%	16%	0.77	79%

To look deeper into the “vegetation” class, Table 5 also shows the results disaggregated by “increase”, “decrease” and “no change” types, with the corresponding overall accuracy and omission/commission errors. As can be seen, for both the increase and decrease in vegetation, around 1 in 4 detections was a false alarm, whereas the percentage of missed changes were 20% and 12%, respectively. It is worth noting that there was no confusion between the two classes, as all the errors fell into the “no change” class. For this class, instead, the commission and omission errors were much lower, namely, 4% and 9%, respectively.

**Table 5.** “Summer classification” (full dataset): detailed confusion matrix for the “vegetation” class.

	Increase	Decrease	No Change	Total	Commission Errors
Increase	8	0	3	11	27%
Decrease	0	51	18	69	26%
no change	2	7	213	222	4%
Total	10	58	234	302	
Omission Errors	20%	12%	9%		OA = 90%

### 3.2.2. Changepoint Classification

The “change point classification” takes into consideration only the RDSs for which at least one change point date has been estimated within the change detection process. As multiple changes can occur in the same site during the considered time period, a yearly comparison was required for each estimated change date. This was only possible using the Pléiades dataset, as only for this ground truth are the exact change dates available. A performance assessment (Tables 6 and 7) was carried out for all the change point dates knowing that the overall accuracy of the change point dates themselves was shown in a previous section.

**Table 6.** “Change point classification” (Pléiades dataset): confusion matrix and performance metrics.

	TP	FP	FN	TN	TPR	FPR	$F_1$ -Score	OA
Vegetation	6	1	3	16	67%	6%	0.75	84%
Building	7	1	3	15	70%	6%	0.78	85%
Soil	11	4	4	7	73%	36%	0.73	69%

**Table 7.** “Changepoint classification” (Pléiades dataset): detailed confusion matrix for the “vegetation” and “building” classes.

Vegetation					
	Increase	Decrease	No Change	Total	Commission Errors
Increase	0	0	0	0	-
Decrease	0	6	1	7	14%
No change	0	3	16	19	16%
Total	0	9	17	26	
Omission Errors	-	33%	6%		OA = 85%
Building					
	Increase	Decrease	No Change	Total	Commission Errors
Increase	2	0	0	2	0%
Decrease	0	5	1	6	17%
No change	2	1	15	18	17%
Total	4	6	16	26	
Omission Errors	50%	17%	6%		OA = 85%

Although some dates were during winter months, the results for the vegetation changes remained good, with an OA of 84% and a  $F_1$ -score of 0.75. With respect to the “summer classification”, the main difference here was in the TPR, which was lower by 20 percentage points (87% for “summer classification” and 67% for Pléiades dataset). As regards the “building” class, there was the opposite trend for the Pléiades dataset, with both a higher OA and  $F_1$ -score than those obtained for the “summer classification”. Although the TPR was slightly lower, the significant drop in the FPR improved the performance. Finally, for the “soil” class, all the metrics showed a drop in the performance, especially as far as the FPR is concerned.

To complete the analysis, the detailed confusion matrices for the classes “vegetation” and “building” are provided in Table 7. Once again, the results are disaggregated by “increase”, “decrease” and “no change” types. For the “vegetation” class, no increase was reported within any site of the ground truth; therefore, no metric was calculated. Instead, out of nine “decrease” changes, six were correctly identified, resulting in a commission error of 14% and an omission error of 33%. If we look at the “no change” class, we had a similar false alarm rate, but a much lower miss rate. For the “building” class, half of the “increase” changes in buildings were missed (50% omission error). However, all the changes that were flagged as an increase were correct (0% commission error). Instead, the classification of a decrease was more accurate, with only one false alarm and one missed detection. Finally, the “no change” classification was the one providing the best performance, with a commission error of 17% and an omission error of 6%.

#### 4. Discussion

The results described in the prior section provide answers to the several challenges that can be encountered when detecting changes on specific sites. Indeed, besides detecting the changes with their dates, there is a need to classify the type of changes and to detect gradual changes. Four main observations may be drawn from this research.

First, the proposed method provided satisfactory results for the change detection and the change classification for both ground truth datasets. As far as the change detection is concerned, thanks to the complementary information provided by the  $\sigma_{VH}$  and NDWI features (the former mainly for buildings, and the latter mainly for vegetation/soil), we were able to achieve an overall accuracy for the full dataset of 79%. As far as the change classification is concerned, the OA ranged from 79% to 90%, depending on the type of change that was considered (vegetation, building and soil). The OA of 90% and the  $F_1$ -score

of 0.80, obtained for the vegetation “summer classification”, illustrate the well-known robustness of the selection of the NDVI as a vegetation indicator [25,49,53], especially in summer conditions. As previously shown in [47], the BAI was proven to be useful for soil detection. Regarding the classification of buildings, the results revealed the suitability of combining the BI, BI2 and SBI indices, as an OA of 76% and an F<sub>1</sub>-score of 0.71 were obtained for the “summer classification”. As mentioned in the Methods section, these indices were not used for the building classification rules of the “changepoint classification” and were replaced by the  $\sigma_{0VH}$  feature. This is due to the fact that the probability of finding cloud-free images in other periods than the summer is lower and the radar backscatter helps improving building discrimination thanks to its sensitivity to variations in height and shape. For this reason, it will be useful to carry out additional tests to investigate whether the use of the  $\sigma_{0VH}$  feature could be used also for the “summer classification”. Moreover, further research could be conducted in regard to the number of Sentinel-2 images used for the “changepoint classification”. Although data gaps were filled in through linear interpolation and the time series were smoothed using a Gaussian kernel, the cloud cover limits the number of usable images, especially during winter months. By only selecting the dates for which a certain number of S2 images are available, it is likely that the performance of the change classification would be improved.

Second, the “summer classification” is better suited for the detection of gradual changes. Figure 6 illustrates an ongoing vegetation growth leading to a soil decrease. This was not captured by the changepoint detection method but was classified as a vegetation increase and soil change thanks to the summer 2016–2018 comparison. The “summer classification” also provided better vegetation classification for change dates that occurred during winter, as seasonality strongly impacts the performance, as most vegetation is dormant during the winter. However, when comparing the “summer classification” and the “changepoint classification” results, it should be taken into account that the size of the two datasets is very different (302 vs. 26), and this had an impact on the results both in terms of representativeness and numerical accuracy.

Third, the use of vector polygons originating from the RDSs vector file to group the image pixels in the change analysis constitutes, at the same time, an advantage and a limitation. The fact that we averaged the information over the whole sites, on the one hand, helped reduce the noise (especially as far as Sentinel-1 is concerned) and filter out unnecessary details, but on the other hand, it may have led to the non-detection and/or non-classification of either small changes or bigger changes occurring on large sites, as the scales of the changes do not always match the scales of the vector polygons [14]. To partially overcome these issues, the polygon size could be reduced, for example, by segmenting each site either based on a fixed grid or external sources, such as WALLonie Occupation et Utilisation du Sol (WALOUS) [54,55]. However, this can lead to other problems, such as a significant increase in the computing power and and/or the creation of a large number of objects that would be too small compared to the Sentinel spatial resolution. Moreover, although external sources could, in principle, provide additional information on the type of change, this leads to the challenge of keeping these data up to date.

Fourth, the use of Sentinel data also has its limitations. First, as mentioned above, the spatial resolution reduces the number of RDSs for which the results can be reliable. For example, in total, 90.4% of the RDSs were larger than 400 square meters (roughly one Sentinel-1 pixel and four Sentinel-2 pixels). Moreover, although most of the sites are former industrial facilities with extensive infrastructure, changes may occur on only minor parts of the site, as illustrated in Figure 7. However, Sentinel images offer major advantages compared to orthophotos, which are open access but provided once a year, or Pléiades images, which can be obtained on demand and are costly. In fact, not only can they guarantee a much higher temporal coverage (especially if we consider the Sentinel-1 all-weather capabilities), but they are also completely free, which means that the operational costs of the tool are significantly reduced. Moreover, thanks to the Terrascope platform and its cloud computing environment, the method is automated and provides, every

two months, results that are directly usable by regional authorities. Although the use of Sentinel data limits the number of RDSs that can be analyzed and the size of the changes detected, thanks to the results that we have shown, the regional authorities will be able to update the RDS inventory in a more efficient and less expensive way. Indeed, the SARSAR service enables the prioritization of the orthophotos analysis work and drastically limits field efforts. Table 8 shows a sample of bimestrial final change lists, and Figure 8 presents four RDSs, three for which a change date was detected and one with no change.

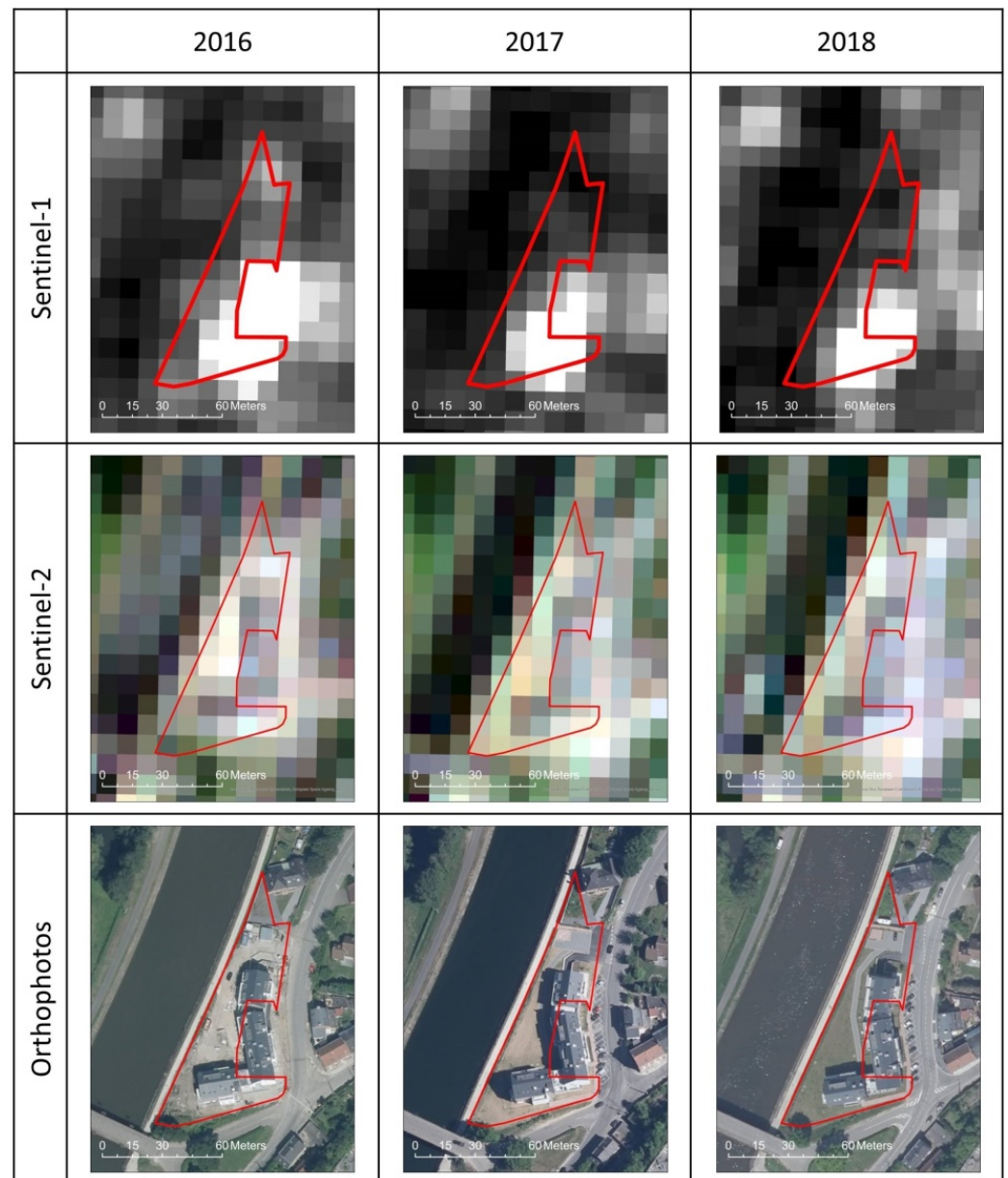


**Figure 6.** Close-ups of an RDS showing gradual vegetation increase (“Ets Biernaux”), between 2016 and 2018, illustrated at the top with Sentinel-1 images, in the middle with Sentinel-2 images and at the bottom with orthophotos.

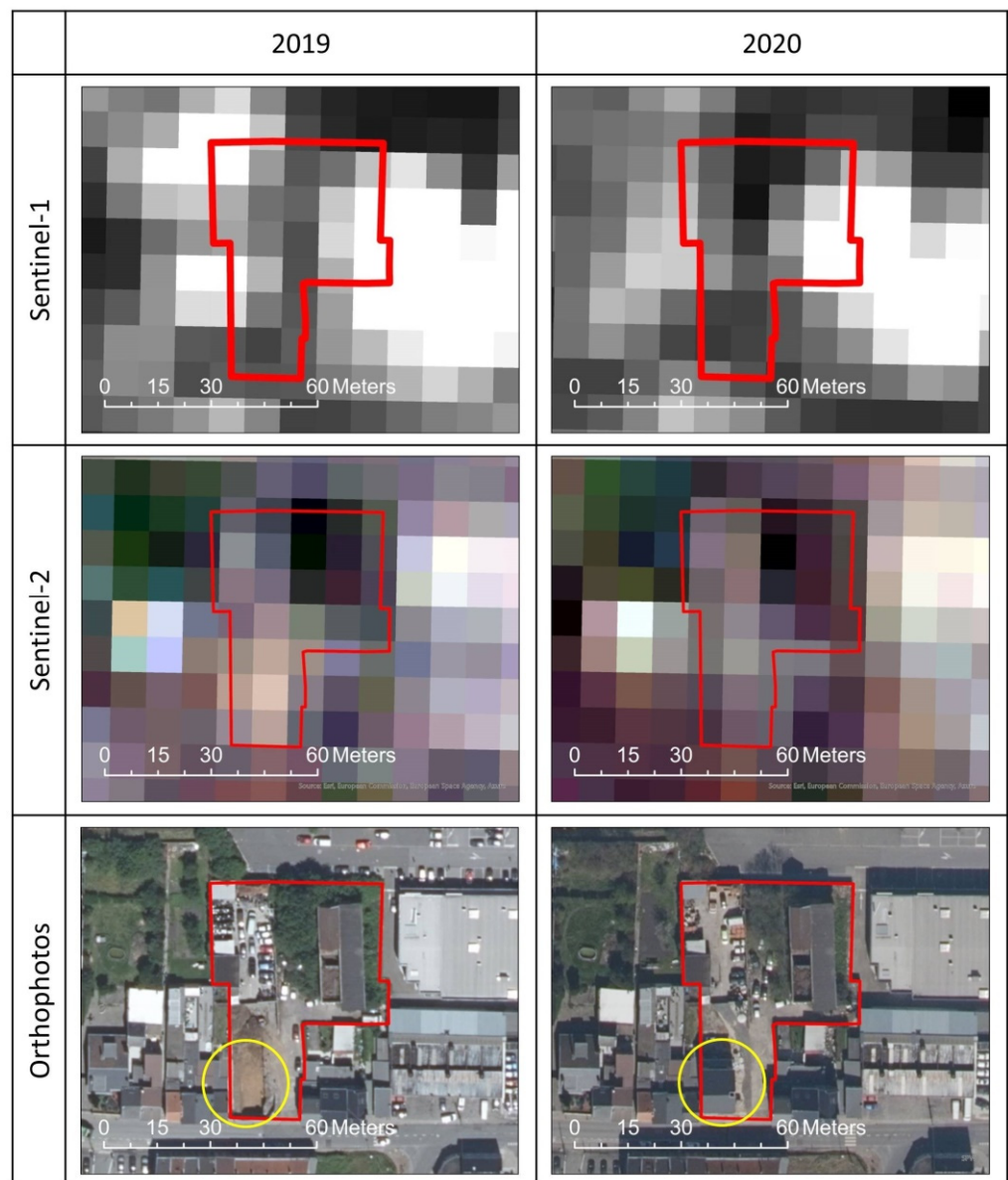


**Figure 7.** Close-ups of an RDS showing a building increase, between 2019 and 2020, too small for the Sentinel spatial resolution (“S.A.N.I. Carrelages”), illustrated at the top with Sentinel-1 images, in the middle with Sentinel-2 images and at the bottom with orthophotos.

**Table 8.** Example of bimestrial final change list for a sample of RDSs.

CODECARTO	RDS Name	Change Date	Estimated Change Date	Vegetation Change	Building Change	Soil Change
52011-ISA-0040-01	Cordial Bowling	Yes	20 April 2020	Yes, decrease	No	Yes
52011-ISA-0110-01	Carsid—Agglomération	Yes	12 March 2019	No	Yes, decrease	Yes
62063-ISA-0073-01	Patience et Beaujonc—site secondaire	Yes	31 March 2020	Yes, decrease	Yes, decrease	Yes
52011-ISA-0003-01	Technopôle de la Villette	No	NA	No	No	No

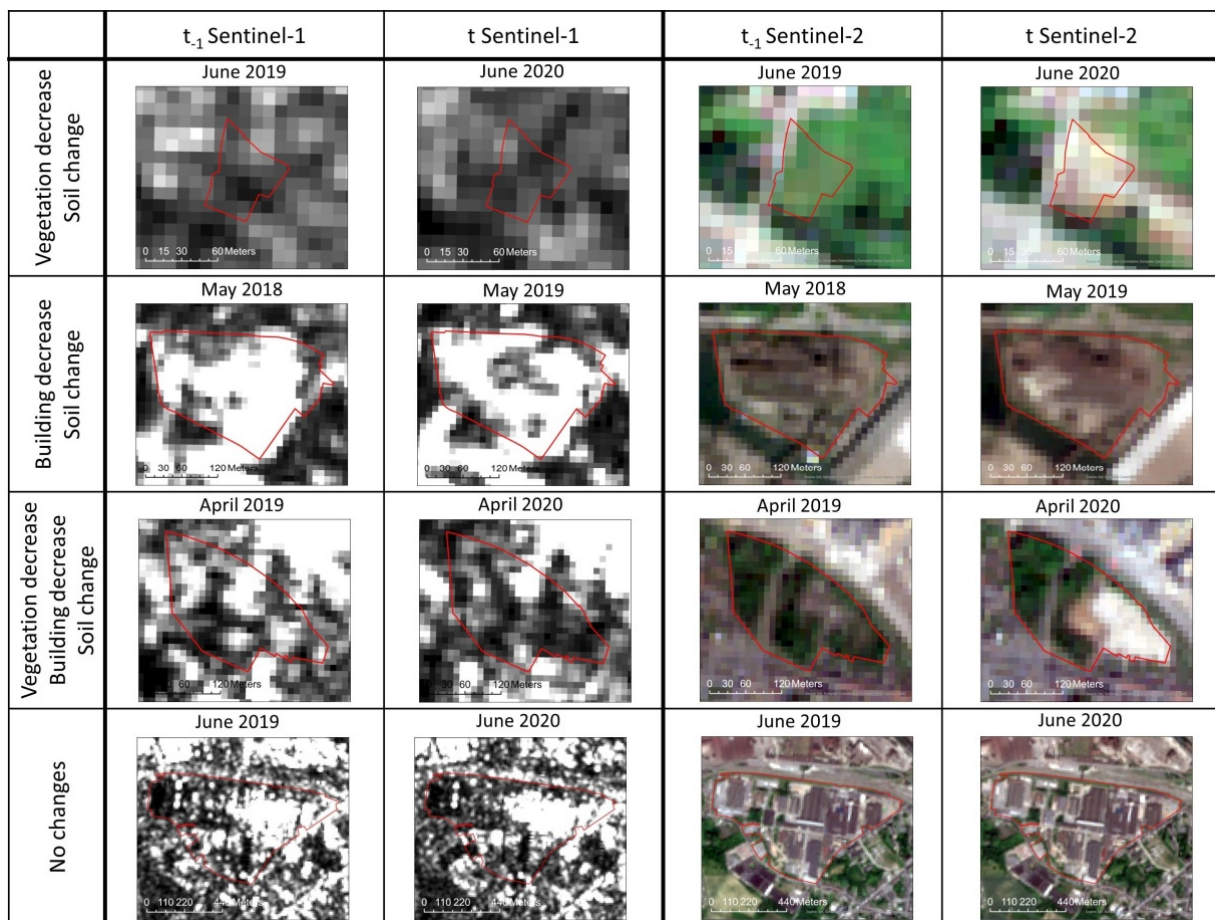


**Figure 8.** Examples of detected and classified changes, on Sentinel-1 images (left) and Sentinel-2 images (right). Details of the changes are explained in Table 8.

## 5. Conclusions

Managing former industrial lands is essential for urban planning and limiting the urbanization of new lands. In this article, we presented SARSAR, a new Earth observation service that has been developed to support the Walloon authorities' daily work by helping them update the RDS inventory in a more responsive, efficient and cost-effective manner.

The SARSAR service exploits Sentinel-1 and Sentinel-2 images, with their high spatial and temporal resolution and open data policy, and the cloud computing environment offered by Terrascope to generate and deliver a change report every two months directly to the Walloon authorities, who can integrate it into their management system. This saves time and effort compared to the current methods of updating the inventory (visual analysis of orthophotos and systematic field visits), enabling personnel to prioritize their work and focus on the RDSs showing evidence of significant changes. This service, which first performs a set of routines to extract and prepare the input data, is composed of two main processes: one for the flagging of the sites that are likely to have changed and one in charge of the classification of the changes.

The performance assessment provided satisfactory results, with an overall accuracy of around 80% for the change detection and in the range 70–90% for the change classification (depending on the class considered). The results highlight the relevance of using Sentinel-1 data, as well as a selection of Sentinel-2 indices, especially the NDVI for vegetation monitoring, and show the complementarity of the two processes in identifying both abrupt and gradual changes.

The results presented in this paper highlight opportunities not only for brownfield monitoring in other regions but also for multiple application domains and a larger user

community, from land management and planning strategies, to agricultural and forestry areas monitoring, through disaster response mapping.

**Author Contributions:** Conceptualization, S.P., M.S., X.N. and E.H.; methodology, S.P., M.S., C.W., G.S., X.N. and E.H.; software, M.S., C.W. and G.S.; validation, S.P. and M.S.; formal analysis, S.P. and M.S.; investigation, S.P. and M.S.; resources; data curation, S.P., M.S., C.W. and G.S.; writing—original draft preparation, S.P.; writing—review and editing, S.P., M.S., C.W. and E.H.; visualization, S.P. and M.S.; supervision, X.N. and E.H.; project administration, S.P., M.S., X.N. and E.H.; funding acquisition, M.S., X.N. and E.H. All authors have read and agreed to the published version of the manuscript.

**Funding:** The research presented in this paper is funded by BELSPO (Belgian Science Policy Office) in the frame of the STEREO III programme—project SR/00/372.

**Data Availability Statement:** Not applicable.

**Acknowledgments:** The authors would like to thank the European Union’s Earth Observation Programme Copernicus and VITO for the provision of the Sentinel images through Terrascope and for the virtual research environments. The authors would like to thank Airbus and BELSPO for the provision of the Pléiades images, and the Service Public de Wallonie for the orthophotos. The authors would also like to thank BELSPO and their STEREO program (Support To Exploitation and Research in Earth Observation). Finally, the authors would like to thank the members of the Remote sensing and geodata unit (ISSeP), in particular Odile Close and Benjamin Beaumont, for their support and paper review.

**Conflicts of Interest:** The authors declare no conflict of interest.

## References

1. Ferber, U.; Tomerius, S. Brownfield redevelopment: Strategies and approaches in Europe and the United States. In *Private Finance and Economic Development: City and Regional Investment*; OECD Publishing: Paris, France, 2003. [CrossRef]
2. Turvani, M.; Tonin, S. Brownfields Remediation and reuse: An opportunity for urban sustainable development. In *Sustainable Development and Environmental Management: Experiences and Case Studies*; Clini, C., Musu, I., Gullino, M.L., Eds.; Springer: Dordrecht, The Netherlands, 2008; pp. 397–411. [CrossRef]
3. Rénover et Réaménagement la Wallonie. Available online: [http://lampspw.wallonie.be/dgo4/site\\_amenagement/site/directions/dao/sarpdf](http://lampspw.wallonie.be/dgo4/site_amenagement/site/directions/dao/sarpdf) (accessed on 27 January 2022).
4. Sites à Réaménager. Available online: [https://www.iweps.be/wp-content/uploads/2021/12/T008-SITES.REAM\\_-122021\\_full1.pdf](https://www.iweps.be/wp-content/uploads/2021/12/T008-SITES.REAM_-122021_full1.pdf) (accessed on 27 January 2022).
5. Service Public de Wallonie, Code du Développement Territorial. Available online: [http://lampspw.wallonie.be/dgo4/tinymvc/apps/amenagement/views/documents/juridique/codt/CoDT\\_Fr.pdf](http://lampspw.wallonie.be/dgo4/tinymvc/apps/amenagement/views/documents/juridique/codt/CoDT_Fr.pdf) (accessed on 27 January 2022).
6. Inventaire des Sites à Réaménager. Available online: [http://lampspw.wallonie.be/dgo4/site\\_sar/index.php](http://lampspw.wallonie.be/dgo4/site_sar/index.php) (accessed on 27 January 2022).
7. Schiller, G.; Blum, A.; Hecht, R.; Oertel, H.; Ferber, U.; Meinel, G. Urban infill development potential in Germany: Comparing survey and GIS data. *Build. Cities* **2021**, *2*, 36–54. [CrossRef]
8. Banzhaf, E.; Netzband, M. Detecting urban brownfields by means of high resolution satellite imagery. The International Archives of the Photogrammetry. *Remote Sens. Spat. Inf. Sci.* **2004**, *35*, 460–466.
9. Ferrara, V. Brownfield identification: Different approaches for analysing data detected by means of remote sensing. *WIT Trans. Ecol. Environ.* **2008**, *107*, 45–54. [CrossRef]
10. Xu, S.; Ehlers, M. Automatic detection of urban vacant land: An open-source approach for sustainable cities. *Comput. Environ. Urban Syst.* **2022**, *91*, 101729. [CrossRef]
11. Atturo, C.; Cianfrone, C.; Ferrara, V.; Fiumi, L.; Fontinovo, G.; Ottavi, C.M. Remote sensing detection techniques for brownfield identification and monitoring by GIS tools. *WIT Trans. Ecol. Environ.* **2006**, *94*, 241–250. [CrossRef]
12. Singh, A. Review Article Digital change detection techniques using remotely-sensed data. *Int. J. Remote Sens.* **1989**, *10*, 989–1003. [CrossRef]
13. Hecheltjen, A.; Thonfeld, F.; Menz, G. Recent advances in remote sensing change detection—A review. In *Land Use and Land Cover Mapping in Europe. Remote Sensing and Digital Image Processing*; Springer: Dordrecht, The Netherlands, 2014. [CrossRef]
14. Tewkesbury, A.P.; Comber, A.J.; Tate, N.J.; Lamb, A.; Fisher, P.F. A critical synthesis of remotely sensed optical image change detection techniques. *Remote Sens. Environ.* **2015**, *160*, 1–14. [CrossRef]
15. Wang, P.; Wang, L.; Leung, H.; Zhang, G. Super-Resolution Mapping Based on Spatial-Spectral Correlation for Spectral Imagery. *IEEE Trans. Geosci. Remote Sens.* **2021**, *59*, 2256–2268. [CrossRef]
16. Shi, W.; Zhang, M.; Zhang, R.; Chen, S.; Zhan, Z. Change Detection Based on Artificial Intelligence: State-of-the-Art and Challenges. *Remote Sens.* **2020**, *12*, 1688. [CrossRef]

17. Khelifi, L.; Mignotte, M. Deep Learning for Change Detection in Remote Sensing Images: Comprehensive Review and Meta-Analysis. *IEEE Access* **2020**, *8*, 126385–126400. [[CrossRef](#)]
18. Yan, J.; Wang, L.; Song, W.; Chen, Y.; Chen, X.; Deng, Z. A time-series classification approach based on change detection for rapid land cover mapping. *ISPRS J. Photogramm. Remote Sens.* **2019**, *158*, 249–262. [[CrossRef](#)]
19. Aminikhanghahi, S.; Cook, D.J. A survey of methods for time series change point detection. *Knowl. Inf. Syst.* **2017**, *51*, 339–367. [[CrossRef](#)] [[PubMed](#)]
20. Francini, S.; McRoberts, R.E.; Giannetti, F.; Mencucci, M.; Marchetti, M.; Scarascia Mugnozza, G.; Chirici, G. Near-real time forest change detection using PlanetScope imagery. *Eur. J. Remote Sens.* **2020**, *53*, 233–244. [[CrossRef](#)]
21. Torres, R.; Snoeij, P.; Geudtner, D.; Bibby, D.; Davidson, M.; Attema, E.; Potin, P.; Rommen, B.; Floury, N.; Brown, M.; et al. GMES Sentinel-1 mission. *Remote Sens. Environ.* **2012**, *120*, 9–24. [[CrossRef](#)]
22. Drusch, M.; del Bello, U.; Carlier, S.; Colin, O.; Fernandez, V.; Gascon, F.; Hoersch, B.; Isola, C.; Laberinti, P.; Martimort, P.; et al. Sentinel-2: ESA's Optical High-Resolution Mission for GMES Operational Services. *Remote Sens. Environ.* **2012**, *120*, 25–36. [[CrossRef](#)]
23. Belgiu, M.; Csillik, O. Sentinel-2 cropland mapping using pixel-based and object-based time-weighted dynamic time warping analysis. *Remote Sens. Environ.* **2018**, *204*, 509–523. [[CrossRef](#)]
24. Woodcock, C.E.; Loveland, T.R.; Herold, M.; Bauer, M.E. Transitioning from change detection to monitoring with remote sensing: A paradigm shift. *Remote Sens. Environ.* **2020**, *238*, 111558. [[CrossRef](#)]
25. Puletti, N.; Bascietto, M. Towards a Tool for Early Detection and Estimation of Forest Cuttings by Remotely Sensed Data. *Land* **2019**, *8*, 58. [[CrossRef](#)]
26. Radoux, J.; Chomé, G.; Jacques, D.C.; Waldner, F.; Bellemans, N.; Matton, N.; Lamarche, C.; D'Andrimont, R.; Defourny, P. Sentinel-2's Potential for Sub-Pixel Landscape Feature Detection. *Remote Sens.* **2016**, *8*, 488. [[CrossRef](#)]
27. Lefebvre, A.; Sannier, C.; Corpetti, T. Monitoring Urban Areas with Sentinel-2A Data: Application to the Update of the Copernicus High Resolution Layer Imperviousness Degree. *Remote Sens.* **2016**, *8*, 606. [[CrossRef](#)]
28. Close, O.; Beaumont, B.; Petit, S.; Fripiat, X.; Hallot, E. Use of Sentinel-2 and LUCAS Database for the Inventory of Land Use, Land Use Change, and Forestry in Wallonia, Belgium. *Land* **2018**, *7*, 154. [[CrossRef](#)]
29. Phiri, D.; Simwanda, M.; Salekin, S.; Nyirenda, V.R.; Murayama, Y.; Ranagalage, M. Sentinel-2 Data for Land Cover/Use Mapping: A Review. *Remote Sens.* **2020**, *12*, 2291. [[CrossRef](#)]
30. Pesaresi, M.; Corbane, C.; Julea, A.; Florczyk, A.J.; Syrris, V.; Soille, P. Assessment of the Added-Value of Sentinel-2 for Detecting Built-up Areas. *Remote Sens.* **2016**, *8*, 299. [[CrossRef](#)]
31. Reiche, J.; Hamunyela, E.; Verbesselt, J.; Hoekman, D.; Herold, M. Improving near-real time deforestation monitoring in tropical dry forests by combining dense Sentinel-1 time series with Landsat and ALOS-2 PALSAR-2. *Remote Sens. Environ.* **2018**, *204*, 147–161. [[CrossRef](#)]
32. Ban, Y.; Yousif, O.; Hu, H. Global urban monitoring and assessment through earth observation: Fusion of SAR and optical data for urban land cover mapping and change detection. In *Global Urban Monitoring and Assessment through Earth Observation*; CRC Press: Boca Raton, FL, USA, 2014.
33. Yousif, O.; Ban, Y. Fusion of SAR and optical data for unsupervised change detection: A case study in Beijing. In Proceedings of the Joint Urban Remote Sensing Event (JURSE), Dubai, United Arab Emirates, 6–8 March 2017.
34. Hirschmugl, M.; Deutscher, J.; Gutjahr, K.; Sobe, C.; Schardt, M. Combined use of SAR and optical time series data for near real-time forest disturbance mapping. In Proceedings of the 9th International Workshop on the Analysis of Multitemporal Remote Sensing Images (MultiTemp), Brugge, Belgium, 27–29 June 2017.
35. Satalino, G.; Mattia, F.; Balenzano, A.; Lovergine, F.P.; Rinaldi, M.; de Santis, A.P.; Ruggieri, S.; Nafria García, D.A.; Paredes Gómez, V.; Ceschia, E.; et al. Sentinel-1 & sentinel-2 data for soil tillage change detection. In Proceedings of the IGARSS 2018—2018 IEEE International Geoscience and Remote Sensing Symposium, Valencia, Spain, 22–27 July 2018.
36. Haas, J.; Ban, Y. Sentinel-1A SAR and sentinel-2A MSI data fusion for urban ecosystem service mapping. *Remote Sens. Appl. Soc. Environ.* **2019**, *8*, 41–53. [[CrossRef](#)]
37. Mercier, A.; Betbeder, J.; Rumiano, F.; Baudry, J.; Gond, V.; Blanc, L.; Bourgoin, C.; Cornu, G.; Ciudad, C.; Marchamalo, M.; et al. Evaluation of Sentinel-1 and 2 Time Series for Land Cover Classification of Forest-Agriculture Mosaics in Temperate and Tropical Landscapes. *Remote Sens.* **2019**, *11*, 979. [[CrossRef](#)]
38. Eckerstorfer, M.; Vickers, H.; Malnes, E.; Grahn, J. Near-Real Time Automatic Snow Avalanche Activity Monitoring System Using Sentinel-1 SAR Data in Norway. *Remote Sens.* **2019**, *11*, 2863. [[CrossRef](#)]
39. Pulvirenti, L.; Squicciarino, G.; Fiori, E.; Fiorucci, P.; Ferraris, L.; Negro, D.; Gollini, A.; Severino, M.; Puca, S. An Automatic Processing Chain for Near Real-Time Mapping of Burned Forest Areas Using Sentinel-2 Data. *Remote Sens.* **2020**, *12*, 674. [[CrossRef](#)]
40. Cerbelaud, A.; Roupioz, L.; Blanchet, G.; Breil, P.; Briottet, X. A repeatable change detection approach to map extreme storm-related damages caused by intense surface runoff based on optical and SAR remote sensing: Evidence from three case studies in the South of France. *ISPRS J. Photogramm. Remote Sens.* **2021**, *182*, 153–175. [[CrossRef](#)]
41. Terrascope. Available online: <https://terrascope.be/en/> (accessed on 27 January 2022).

42. Everaerts, J.; Clarijs, D. Terrascope enables geohazard monitoring using the sentinel satellite constellation. In Proceedings of the 2021 IEEE International Geoscience and Remote Sensing Symposium IGARSS, Brussels, Belgium, 11–16 July 2021; pp. 1895–1898. [\[CrossRef\]](#)
43. Killick, R.; Fearnhead, P.; Eckley, I. Optimal detection of changepoints with a linear computational cost. *J. Am. Stat. Assoc.* **2012**, *107*, 1590–1598. [\[CrossRef\]](#)
44. Stasolla, M.; Petit, S.; Wyard, C.; Swinnen, G.; Neyt, X.; Hallot, E. Urban sites change detection by means of sentinel-1 and sentinel-2 time series. In Proceedings of the IEEE IGARSS'21, Brussels, Belgium, 11–16 July 2021; pp. 1065–1068.
45. Asokan, A.; Anitha, J. Change detection techniques for remote sensing applications: A survey. *Earth Sci. Inform.* **2019**, *12*, 143–160. [\[CrossRef\]](#)
46. Hussain, M.; Chen, D.; Cheng, A.; Wei, H.; Stanley, D. Change detection from remotely sensed images: From pixel-based to object-based approaches. *ISPRS J. Photogramm. Remote Sens.* **2013**, *80*, 91–106. [\[CrossRef\]](#)
47. Bouziani, M.; Goïta, K.; He, D.C. Automatic change detection of buildings in urban environment from very high spatial resolution images using existing geodatabase and prior knowledge. *ISPRS J. Photogramm. Remote Sens.* **2010**, *65*, 143–153. [\[CrossRef\]](#)
48. Escadafal, R. Remote sensing of arid soil surface color with Landsat thematic mapper. *Adv. Space Res.* **1989**, *9*, 159–163. [\[CrossRef\]](#)
49. Tucker, C.J. Red and Photographic Infrared Linear Combinations for Monitoring Vegetation. *Remote Sens. Environ.* **1979**, *8*, 127–150. [\[CrossRef\]](#)
50. McFeeters, S.K. The use of the Normalized Difference Water Index (NDWI) in the delineation of open water features. *Int. J. Remote Sens.* **1996**, *17*, 1425–1432. [\[CrossRef\]](#)
51. Gadal, S.; Ouerghemmi, W. Multi-Level Morphometric Characterization of Built-up Areas and Change Detection in Siberian Sub-Arctic Urban Area: Yakutsk. *ISPRS Int. J. Geo-Inf.* **2019**, *8*, 129. [\[CrossRef\]](#)
52. Réjichi, S.; Chaabane, F.; Tupin, F. Expert Knowledge-Based Method for Satellite Image Time Series Analysis and Interpretation. *IEEE J. Sel. Top. Appl. Earth Obs. Remote Sens.* **2015**, *8*, 2138–2150. [\[CrossRef\]](#)
53. Lunetta, R.S.; Knight, J.F.; Ediriwickrema, J.; Lyon, J.G.; Worthy, L.D. Land-cover change detection using multi-temporal MODIS NDVI data. *Remote Sens. Environ.* **2006**, *105*, 142–154. [\[CrossRef\]](#)
54. Bassine, C.; Radoux, J.; Beaumont, B.; Grippa, T.; Lennert, M.; Champagne, C.; de Vroey, M.; Martinet, A.; Bouchez, O.; Deffense, N.; et al. First 1-M Resolution Land Cover Map Labeling the Overlap in the 3rd Dimension: The 2018 Map for Wallonia. *Data* **2020**, *5*, 117. [\[CrossRef\]](#)
55. Beaumont, B.; Grippa, T.; Lennert, M. A user-driven process for INSPIRE-compliant land use database: Example from Wallonia, Belgium. *Ann. GIS* **2021**, *27*, 211–224. [\[CrossRef\]](#)